

Brain hothubs and dark functional networks: Correlation analysis between amplitude and connectivity for Broca's aphasia

Feng Lin^{1,2}, **Shao-Qiang Cheng**³, **Dong-Qing Qi**⁴, **Yu-Er Jiang**¹, **Qian-Qian Lyu**¹, **Li-Juan Zhong**¹, **Zhong-Li Jiang**
Corresp. 1, 2

¹ Department of Rehabilitation Medicine, The First Affiliated Hospital of Nanjing Medical University, Nanjing, Jiangsu, China

² Department of Rehabilitation Medicine, The Affiliated Sir Run Run Hospital of Nanjing Medical University, Nanjing, Jiangsu, China

³ Department of Neurology, The First People's Hospital of Xianyang, Xianyang, Shanxi, China

⁴ The First Affiliated Hospital of USTC, Division of Life Sciences and Medicine, University of Science and Technology of China, Hefei, Anhui, China

Corresponding Author: Zhong-Li Jiang
Email address: jiangzhongli@njmu.edu.cn

Source localization and functional brain network modeling are methods of identifying critical regions during cognitive tasks. The first activity estimates the relative differences of the signal amplitudes in regions of interest (ROI) and the second activity measures the statistical dependence among signal fluctuations. We hypothesized that the source amplitude-functional connectivity relationship decouples or reverses in persons having brain impairments. Five Broca's aphasics with five matched cognitively healthy controls underwent overt picture-naming magnetoencephalography scans. The gamma-band (30–45 Hz) phase-locking values were calculated as connections among the ROIs. We calculated the partial correlation coefficients between the amplitudes and network measures and detected four node types, including hothubs with high amplitude and high connectivity, coldhubs with high connectivity but lower amplitude, non-hub hotspots, and non-hub coldspots. The results indicate that the high-amplitude regions are not necessarily highly connected hubs. Furthermore, the Broca aphasics utilized different hothub sets for the naming task. Both groups had dark functional networks composed of coldhubs. Thus, source amplitude-functional connectivity relationships could help reveal functional reorganizations in patients. The amplitude-connectivity combination provides a new perspective for pathological studies of the brain's dark functional networks.

Brain Hothubs and Dark Functional Networks: Correlation Analysis Between Amplitude and Connectivity for Broca's Aphasia

Feng Lin^{1,2}, Shao-Qiang Cheng³, Dong-Qing Qi⁴, Yu-Er Jiang¹, Qian-Qian Lyu¹, Li-Juan
Zhong¹, Zhong-Li Jiang^{1,2}

1 Department of Rehabilitation Medicine, The First Affiliated Hospital of Nanjing Medical
University, Nanjing, 210029, P.R.China.

2 Department of Rehabilitation Medicine, The Affiliated Sir Run Run Hospital of Nanjing
Medical University, Nanjing, 210000, P.R.China.

3 Department of Neurology, The First People's Hospital of Xianyang, Xianyang, 712000,
P.R.China.

4 The First Affiliated Hospital of USTC, Division of Life Sciences and Medicine, University of
Science and Technology of China, Hefei, Anhui, 2300001, P.R.China

Corresponding Author:

Zhongli JIANG^{1,2}

No.300, Guangzhou Road, Gulou District, Nanjing, 210029, P.R.China.

Email address: jiangzhongli@njmu.edu.cn

Abstract

Source localization and functional brain network modeling are methods of identifying critical regions during cognitive tasks. The first activity estimates the relative differences of the signal amplitudes in regions of interest (ROI) and the second activity measures the statistical dependence among signal fluctuations. We hypothesized that the source amplitude–functional connectivity relationship decouples or reverses in persons having brain impairments. Five Broca’s aphasics with five matched cognitively healthy controls underwent overt picture-naming magnetoencephalography scans. The gamma-band (30–45 Hz) phase-locking values were calculated as connections among the ROIs. We calculated the partial correlation coefficients between the amplitudes and network measures and detected four node types, including hothubs with high amplitude and high connectivity, coldhubs with high connectivity but lower amplitude, non-hub hotspots, and non-hub coldspots. The results indicate that the high-amplitude regions are not necessarily highly connected hubs. Furthermore, the Broca aphasics utilized different hothub sets for the naming task. Both groups had dark functional networks composed of coldhubs. Thus, source amplitude–functional connectivity relationships could help reveal functional reorganizations in patients. The amplitude–connectivity combination provides a new perspective for pathological studies of the brain’s dark functional networks.

Introduction

In functional brain-imaging studies, there are two strategies can be utilized to identify a brain region as a responsible position for a certain task (e.g., picture naming) or event (e.g., seizure) (Youssofzadeh & Babajani-Feremi, 2019; van den Heuvel & Sporns, 2013; Daffertshofer & van Wijk, 2011; Michel & Brunet, 2019; Biswal, 2012; Raichle, 2006; Salmelin, Hari, Lounasmaa, & Sams, 1994). The first strategy utilizes source localization to, for example, find activations that can be quantified by measurements, such as blood-oxygen-level-dependent signals detected through functional magnetic resonance imaging (fMRI) or current densities estimated via electroencephalography or magnetoencephalography (MEG) (Bassett, Khambhati, & Grafton, 2017; Bassett & Sporns, 2017; De Vico Fallani, Richiardi, Chavez, & Achard, 2014; Lewis, 2009). The second strategy utilizes connectivity estimation to, for example, calculate connections that represent statistical dependencies, such as synchronizations or causal relationships among brain regions (Farahani, Karwowski, & Lighthall, 2019; Medaglia, 2017; Bassett & Sporns, 2017; Friston, 2011; Lewis, 2009; O. Sporns, 2002). It is possible to detect

statistical dependencies among regions regardless of whether the regions are highly activated. This yields an inevitable but not fully understood question regarding the relationship between “amplitude” and “connectivity.”

In functional brain imaging, brain regions having large amplitudes are usually exhibited as hotspots, and other low-amplitude regions are considered coldspots. Considering this visualization tradition, van den Heuvel and Sporns (2013) raised a question of whether or not the highly connected functional hubs were potential hotspots for developing diagnostic biomarkers or therapeutic targets. If we view the relationships between amplitude (i.e., hotspots and coldspots) and connectivity (i.e., hubs and non-hubs), there are four possible types of brain regions, including hothubs, coldhubs, non-hub hotspots, and non-hub coldspots. Hassan et al. (2015) reported that the deletion of regions of interest (ROI) having no more than 50% of the highest activations removed the temporal lobe from the brain networks of picture naming. Their findings implied that there were potential coldhubs in functional brain networks and that the possible contribution of “low-energy” regions should be further studied.

To the best of our knowledge, the relationship between activation and functional connectivity remains unexplored regarding task-related functional brain imaging. Few studies have investigated whether highly activated regions are also hubs in the task-related brain network. There are also limited reports of the pathological changes of activation-connectivity relations, and whether non-trivial activation-connection relations exist. In this study, we **hypothesize that** activation–connection coupling patterns exist for the performance of a naming task (i.e., significantly negative or positive correlations by healthy persons). We also **propose that** persons having post-stroke aphasia also have uncoupling patterns or opposite coupling patterns compared with healthy persons. The term “**coupling**” means that there is a significant correlation. The term “**uncoupling**” means there is a non-significant correlation. The term “**opposite coupling**” means that both correlations are significant, but their coefficients have a different sign. Based on a picture-naming task requiring MEG scanning, we investigate whether the highly connected regions are associated with low or high amplitudes. This allows detection of regions having both high activations and critical positions in brain networks (viz., hothubs). Moreover, we also explore the subnetworks comprising the coldhubs. Because such subnetworks are shown as dark parts in functional brain imaging, we call them **dark functional networks**.

Materials & Methods

Five male persons having Broca’s aphasia were recruited from the Rehabilitation Medical Center of the First Affiliated Hospital of Nanjing Medical University. The inclusion criteria were

as follows: (1) a single left-hemisphere stroke confirmed by computed tomography or magnetic resonance imaging (MRI); (2) Broca's aphasia determined by the Mandarin version of the Western Aphasia Battery (WAB); and (3) native right-handed speakers of mandarin Chinese. The exclusion criteria were as follows: (1) severe vision or hearing impairment; (2) any neurological or psychiatric complications other than stroke, including but not limited to the diagnosis of mild cognitive impairment or dementia before stroke; and (3) contradictions with MRI testing. Five healthy volunteers (four males and one female) were enrolled in the control group. All participants performed the picture-naming task in a single session. The demographics are listed in **Table 1**. All participants signed an informed consent form that was approved by the Ethics Committee of The First Affiliated Hospital of Nanjing Medical University (No.2011-SRFA-025). All examinations were carried out under the guidance of the Declaration of Helsinki. Before the MEG test, all participants completed the WAB, which includes spontaneous speech, auditory comprehension, repetition, and naming tasks. The WAB suggests aphasia diagnosis for an aphasia quotient (AQ) <93.8. The WAB results can also be used to categorize the aphasia into different subtypes, such as Broca's or Wernicke's aphasia. All stroke participants in our study were diagnosed with Broca's aphasia.

Experiment paradigm

The participants lay supine on the MEG scanner bed. A set of pictures was randomly presented onto a screen for the naming task. The stimuli consisted of 40 black-and-white outline drawings presented on a white background (see *Supplementary File S1*). They were from the 100 words of the Kent–Rosanoff word association test (Kent & Rosanoff, 1910). All selected stimuli were a picturable noun or had a noun part of the meaning. They were both emotionally neutral and with high frequency (Wang, Bing, & Hou, 2010). We modified a previously reported delayed naming task (Laganaro, Morand, Schwitter, Zimmermann, & Schnider, 2008) based on the paradigm of Levelt et al. (Levelt, Praamstra, Meyer, Helenius, & Salmelin, 1998). Before the experiment, participants were trained to name aloud each picture correctly. This was done to confirm that the participants could perform the naming task in the scanning session (Ellis, Burani, Izura, Bromiley, & Venneri, 2006). Each trial comprised the following procedures (**Figure 1**): a picture was shown on the screen for 200 ms, followed by a blank white screen for 1000 ms. Next, a white question mark on a black background was shown for 2,000 ms. This was followed by a 1,000 ms black interval preceding the next trial. During the target-picture presentation, the participants were expected to perform overt naming. The question mark was a warning for the participants, indicating that they would soon be expected to perform overt

121 naming. The 40 stimuli were randomly arranged as a sequence. The original design of this study
 122 was to let the participants do three runs in each experiment, and each run completed the
 123 sequence. However, our preliminary test showed that the patients could not tolerate a long test
 124 procedure, particularly when they were required to stay alone in a closed room without any tasks,
 125 waiting for the next run. We finally allowed all the participants to execute only a run of 100 trials
 126 (i.e., two-and-a-half sequences). There were no close distances of the same pictures in the run.
 127 The voices were transmitted outside the shielded room via a plastic tube and were recorded by
 128 researchers. The records were then classified as correct responses (i.e., target word or suitable
 129 alternatives) and incorrect responses (i.e., no-response or unsuitable words), according to the
 130 works of Feng Lin, Shao-Qiang Cheng, and Dong-Qing Qi. Only the consensuses would then
 131 become the final decisions. Then, the trials having correct responses were selected for further
 132 analyses.

134 Data acquisition

135 Using a CTF-275 whole-head MEG scanner (VSM Canadian Medical Technology
 136 Company), available from the MEG Center of the Affiliated Brain Hospital of Nanjing Medical
 137 University, raw files of magnetic fields were recorded within the 0.03–100-Hz band. The sample
 138 rate was 1,200 Hz. The participants lay relaxed with their heads fixed under the sensory matrix.
 139 They were trained to avoid limb movements, head movements, and frequent blinking during the
 140 test. The pictures were delivered in a pseudorandom sequence using BrainX6.0 (Cincinnati
 141 Children's Hospital Medical Center, OH, USA) (Dinga et al., 2018; Xiang, Wilson, Otsubo, Ishii,
 142 & Chuang, 2001). The pictures were projected through an aperture onto a mirror, which, in turn
 143 projected the beam onto a screen. The horizontal and vertical visual angles were 3–4° and 1–2°,
 144 respectively. The space between the screen and the nasion of each participant was adjusted to a
 145 comfortable distance of 35–45 cm. The head positions were measured at the beginning and end
 146 of each session. Trials exhibiting motions greater than 0.5 cm were excluded.

147 After the MEG test, the participants underwent an MRI session for lesion delineation and
 148 source localization. The MRI data were acquired on a Signa (GE Medical Systems, USA) 1.5-T
 149 scanner capable of producing a high-resolution T1-weighted anatomical volume image (TR: 33
 150 ms; TE: 9 ms; recording matrix: 256×256 pixels; excitation: 1; the field of view: 240 mm; and
 151 slice thickness: 1.4 mm). Transformation of the MEG coordinate system into MRI-defined space
 152 was achieved with the aid of three fiduciary points marked on the nasion and the right and left
 153 pre-auricular points with MRI markers, which were identical to the positions of the coils used in
 154 the MEG.

Data processing

Brainsuite18a was used for MRI segmentation. Cortical surfaces were extracted from the T1 MRI data. The surface and volume registration was established based on the USCBrain Atlas, which has a total of 65 cortical regions per hemisphere (i.e., the cortex has 130 **original scouts**) (see *Supplementary Table S1*) (Joshi et al., 2017). The anatomic data, including the MRI results and the registered surface files with their corresponding MEG data, were imported into Brainstorm (Tadel et al., 2019; Baillet, 2017; Tadel, Baillet, Mosher, Pantazis, & Leahy, 2011). The recordings were preprocessed using DC-offset correction, linear trend removal, 1–45-Hz band-pass filtering, and 50-Hz notch filtering. Artifacts were detected via signal-space projection and independent component analysis. The raw MEG files were epoched from –200 to 600 ms with a reduced sample rate of 600 Hz. As shown in **Figure 1**, the epoched time window contained the word generation stages rather than the overt speaking actions. The pronouncing periods were only used to ensure that the participants paid attention to and were involved in the task. Although the control participants produced correct responses for all trials, the aphasics had incorrect responses. After discarding the bad trials having incorrect responses or unremovable artifacts, we uniformly resampled the trails into 60 correct ones for each participant for further analyses of the source-space functional connectivity. Although there were repetitions of some pictures, all participants provided corresponding trails during the run. Source reconstruction was performed using weighted minimum-norm estimation (WMNE) on a current density map and constrained dipole orientations (Hincapié et al., 2017). Each original scout was subdivided into six sub-regions. The final subdivided atlas had 776 **refined scouts**. Trials were averaged on the source level for each person using the weighted arithmetic average. The source data for each person were projected onto the USCBrain_BrainSuite_2017 template. We further averaged the projected source files on the group level, finally obtaining one source file per group. Following the previous work of Hassan et al. (2015), we extracted six picture-naming stages: t1 (0–119 ms, visual feature extraction); t2 (120–150 ms, object recognition); t3 (151–190 ms, memory access); t4 (191–320 ms, semantic processing); t5 (321–480 ms, phonological encoding); and t6 (481–535 ms, articulation). Phase-locking values (PLV) among the 776 refined scouts were estimated for each stage on the gamma frequency band of 30–45 Hz. As reported by Hassan et al. (2015), to reduce confounding factors from correlations of adjacent regions, all PLVs were normalized by the mean and standard deviation matrix of the baseline (–200ms–0ms) time-window.

Graph modeling

We use graph theory terminology (de Nooy, Mrvar, & Batagelj, 2018) and the expressions from the work of Rubinov and Sporns (2010) for brain network analyses. A node is a scout of the brain region, and an edge is an undirected line. Size refers to the number of nodes in a network. A cluster refers to a subnetwork of the entire network. In this study, the nodes were the 776 refined scouts, and the edge weights were normalized PLV scores larger than 1.96. We established six undirected refined networks on the subdivided USCBrian Atlas for each person. These personal networks were utilized for further within-subjects and inter-group permutation t-tests. We also established refined networks on the averaged source files for each group. These averaged original networks were applied for further hothub and coldhub detection. The amplitude of each refined scout was measured according to the estimated electric density in a physical unit of picoampere. The scouts were partitioned using a functional scheme (see *Supplementary Table S1*) that included eight systems (Muldoon et al., 2016; Gu et al., 2015): 1) frontoparietal, 2) medial default mode, 3) visual, 4) ventral temporal association, 5) attention, 6) cingulo-opercular, 7) motor and somatosensory, and 8) auditory. By partitioning the functional systems into the left and right hemispheres, the final scheme contained 16 functional modules. In our descriptions, the term “strongly connected” indicates the weight strength of connections. The term “highly connected” is known as the number of connections. The term “heavily connected” implies to the measures concerning both weights and numbers of connections. The term “highly activated” identifies the amplitude of a node.

Network thresholding

To find nontrivial functional connections and get robust findings, Hassan and Wendling (2018) suggested the reduction of the edges in a graph using a series of threshold values. In this work, we utilized the island decomposition technique embedded in Pajek 5.07 to perform fast thresholding operations (Mrvar & Batagelj, 2016). Pajek is a network analysis software package that can achieve fast speed and memory-efficient calculations for large and densely structured graphs (Pavlopoulos, Paez-Espino, Kyrpides, & Iliopoulos, 2017). The island decomposition defines an island as a cluster with highly weighted within-cluster edges. In particular, the weights inside the cluster must be larger than the weights to neighboring nodes outside the cluster. Pajek called for two inputs to control the island thresholding processes: the minimum and maximum island sizes. In this study, the former was fixed to three. This is the minimum graph size that can support calculating clustering coefficients. We shifted the maximum size from 50 to 750 in increments of 50. Given the half nodes of each hemisphere and the total nodes of the entire network, we also set 388 and 776 as candidate maximum island sizes. These numbers determined

the possible size of the main components in the obtained networks. At each naming stage, the island decomposition generated a series of m -island graphs (where m denotes the maximum island size).

Graph measures

The refined networks and their thresholded networks were weighted undirected graphs lacking loops and multiple edges. Based on these graphs, we calculated nine variables for each node (de Nooy et al., 2018; Olaf Sporns, 2016; Rubinov & Sporns, 2010).

The first six variables were calculated without utilizing the network partitions of the 16 functional modules. The **degree centrality** of a node in its weighted definition is the sum of the edge weights connected to the node. This is a measure of the strength of the node in the range of its firstly connected neighbors. The largely weighted degree centrality indicates that the node is heavily connected. The **betweenness centrality** of a node in its weighted definition is the number of weighted shortest paths going through it. This is a measure of the key connector role of the node in transferring information or its role as a bottleneck in blocking information flowing through the graph paths. **Transitivity** is the probability that the first-connected neighbors of a node are also connected. Barrat et al. (Barrat, Barthelemy, Pastor-Satorras, & Vespignani, 2004) reported that the weighted definition of transitivity was the local clustering coefficient having constant edge weights between the target and adjacent nodes. The **k -coreness** of a node was derived from a thresholding method called the “ k -core decomposition”. This method reduces the graph to a maximal subgraph in which each node has at least a degree, k . A valid k -coreness means that a node belongs to the k -core but not to the $(k+1)$ -core, and the k -coreness measures whether a node involves the highly connected core of the brain graph. The **Laplacian centrality** is a measure that concerns the possible destructive effects of deactivating or deleting a node from a graph (Qi et al., 2013). The higher the Laplacian centrality of a node, the more indispensable it is. Note that the k -coreness and Laplacian centrality algorithms do not consider the edge weights. Finally, the **eigenvector centrality** of a node is assigned based on whether the node connects to many other nodes and/or to highly connected nodes. Highly scored nodes are highly connected with highly connected neighbors. That is, they are hubs of the graph (de Nooy et al., 2018). Weighted definitions were applied to the eigenvector centralities obtained in this study.

To measure the distribution of a node’s connections across modules, we also calculated three variables that depend on the network partitions. We used 16 functional modules, as detailed in *Supplementary Table S1*. The **participation coefficient** of a node measures the distribution of its inter-modular connections. If a node is only connected to nodes in the same module, the

participation coefficient is zero. If the node is equally connected to all other modules, the participation coefficient is one. The **gateway coefficient** of a node refers to both its inter-modular and within-modular connections (Vargas & Wahl, 2014). If a node links to the hub within its module and occupies most of the outer connections from other modules to its module, this node has a larger gateway coefficient. As described by Vargas and Wahl (2014), this coefficient makes it feasible to identify nodes with unique inter-modular connections. The **within-module-degree z-score** of a node is its normalized number of edges that connect to other nodes in the same module of the target node.

In this work, all graph measures were calculated using the undirected definitions (Hassan & Wendling, 2018; Rubinov & Sporns, 2010). The degree, betweenness, transitivity, *k*-coreness, and eigenvector centrality were calculated using the igraph 1.2.4.1 package (Csardi & Nepusz, 2006) of the R software. The Laplacian centrality was calculated using Pajek 5.07 (Mrvar & Batagelj, 2016). The within-module-degree z-score, participation coefficient, and gateway coefficient were obtained using the brainGraph 2.2.0 package (Watson, 2019) of the R software.

Hub and hotspot detection

The z-scores of the amplitudes were calculated for both subdivided and original scouts by comparing the baseline of −200 ms. At each stage, the refined scouts were categorized into hotspots or coldspots depending on whether their amplitudes were larger than the mean plus standard deviation (Hassan et al., 2015). The network hubs were detected using Pajek 5.07. As defined by de Nooy et al. (2018), hubs are nodes with top-level eigenvector centralities. However, there is no optimal strategy to determine the top-level cutoff value. In this study, the number of hubs was set to the number of hotspots in each graph. This is an arbitrary selection that includes 11.86%-16.37% nodes. This strategy followed a rule of thumb (de Nooy et al., 2018) and did not exceed the arbitrary threshold of 30% (Youssofzadeh & Babajani-Feremi, 2019). Finally, all nodes were categorized into four types: **hothubs**, **coldhubs**, non-hub coldspots, and non-hub hotspots.

Statistical analysis

Figure 2 shows the data-processing workflow. Inter-group permutation t-tests for the amplitude z-scores on the 130 scouts at each naming stage were processed using Brainstorm (Tadel et al., 2019, 2011), with $p < 0.05$ as the level of significance. Within-subject Pearson coefficients were calculated between the amplitude (i.e., electric densities in a unit of picoamperes) and each of the graph measures on the refined 776 scouts. These were partial

correlations with the effect of subjects removed. Thus, the individuals were regarded as a third variable that should be adjusted when comparing the amplitude with a graph measure. The 95% confidence intervals and significances of the Pearson coefficients were estimated using the psych 1.8.12 package (Revelle, 2019) of the R software. To explore the entire continuum of m-island graphs and select an optimal m value, we plotted all coefficients on a coordinate system for which the x-axis denoted the maximum island size (see *Supplementary Figures S1, S2*). The left pole included m-island graphs having small but strongly connected clusters (i.e., the “rich-club” structures). The right pole contained m-island graphs having both large and highly connected clusters (i.e., large island structures with a wide range of edge weights from weak to strong). If a correlation were significant ($p < 0.05$), it could be regarded as a **coupling correlation**. Conversely, a non-significant correlation could be termed an **uncoupling correlation**. We also did a permutation test on inter-group correlation coefficients with 1,000 randomizations by shuffling the group assignments of individuals [i.e., the 10 individuals in a permutation were randomly reassigned into two groups (5 ones per group) without replacement]. For each permutation, an inter-group difference value of partial correlation coefficients were calculated. The 1,000 values formed an estimation for the distribution of inter-group differences. The statistics of correlation coefficients followed the estimation approach with 95% confidence intervals (Calin-Jageman & Cumming, 2019). The brain networks were visualized using Pajek 5.07 (Mrvar & Batagelj, 2016) and VOSviewer 1.6.13 (van Eck & Waltman, 2009).

Results

Amplitude–connectivity analysis

Figures 3 and 4 show the Pearson correlation coefficients between the ROI amplitudes and their graph measures, for measures independent of and dependent on the brain modules, respectively. A positive significant coefficient suggests that the regions having higher activation levels tend to have high values of the corresponding graph measure. That is, hotter spots occupy pivotal network positions. Conversely, a negative significant coefficient suggests that the regions having lower activation levels tend to have high values of the corresponding graph measure (i.e., colder spots are positioned at important network locations). **Figure 3** shows coefficients in m776-islands, and **Figure 4** shows coefficients in m388-islands. The selection of m values in the two figures was determined by methods summarized in *Supplementary Figures S1, S2*. There are two positions on the x-axis that optimally separate the inter-group distribution of coefficients (see vertical dashed lines in *Supplementary Figures S1, S2*). *Supplementary Figures S3 and S4*

support the significant inter-group differences of Pearson coefficients by showing the 95% confidence intervals of 1,000 random permutations.

Figures 3 and 4 provide two obvious findings. First, the healthy controls had positive significant coefficients, especially at t4, t5, and t6 (**Figure 3**). Second, the coefficients of the two groups deviated from each other with two types of deviation. For Type-I, the two groups had significant but opposite coefficients (i.e., there was a deviation between the two coupling correlations, and the degree results for t4 and 5 are shown in **Figure 3**). For Type-II, one group had significant coefficients, but the other group showed no correlation significance (i.e., the coupling and uncoupling correlations differed, and the degree results for t1, t3 and t6 are shown in **Figure 3**). For the Broca-group view results, Type-I means that significant differences in amplitude–connectivity patterns were noted between the Broca aphasics and the control group, and the Type-II deviation implies emergence or vanishing of amplitude–connectivity patterns in the Broca group.

In **Figure 3**, Stages t4 (semantic processing) and t5 (phonological encoding): the degree, transitivity, *k*-coreness, and Laplace show Type-I deviation with positive significant coefficients in the Broca group. Type-I deviations having positive coefficients in the Broca group occurred at t1 of the eigenvector, t2 of the transitivity, *k*-coreness, Laplace, and eigenvector, t3 of the *k*-coreness, Laplace, and eigenvector, t5 of the betweenness, and t6 of the eigenvector. Type-I deviations having negative coefficients in the Broca group occurred at t1 and t3 of the degree, t1 of the transitivity, *k*-coreness, and Laplace. Type-I deviations having positive coefficients in the control group occurred at t4 and t6 of the betweenness. Type-I deviations having negative coefficients in the control group occurred at t4 of the eigenvector, and t6 of the transitivity, *k*-coreness, and Laplace. In **Figure 4**, within-module-degree z-score shows no significant correlations for each group. The t1, t2, and t3 show significant positive correlations in the Broca group. The t3, t4, t5, and t6 show a significant negative correlation in the control group.

Hotspot and hothub analysis

Although there were different possible categories for the six subdivided scouts in the same 130 original ones, we reported the hothubs on the level of the original 130 scouts (**Figure 5**) if there was at least one hothub on the level of the 776 subdivided scouts. This was because most previous reports did not interpret functional brain activities on a resolution as did the level of the 776 refined scouts (as shown in *Supplementary Table S2*). Therefore, **Figure 5** reports the regions in which hothubs occurred. We also marked eight functional systems in this figure using different colors. As detailed in **Figure 5**, the Broca group scores for InfOcciGyr_VenPst_R

(right inferior occipital gyrus ventroposterior), PreCune_Sup_R (right precuneus superior), and MidOcciGyr_DsoAnt_L (left middle occipital gyrus dorsal anterior) had significantly lower amplitude z-scores (cells with superscript a). However, they remain in the list of hothubs. Compared with the control group, the Broca group did not use the cingulo-opercular hothubs (yellow cells) across all stages, and the hothubs in the medial default mode (green cells) were absent at t3. They required more visual system regions at each stage (white cells) and resorted to the attention system in the last three stages (pink cells). For the control-group t4 and the Broca-group t5, most hothubs were from the frontoparietal system.

Brain network visualizations

We visualized the m776 islands by showing their hotspots and hubs. **Figure 6** provides a visualization of the brain networks for the semantic processing stage of t4. This figure presents two aspects of the brain networks by changing the node size according to both amplitude and linking strengths. Four colors are used in this figure: red (hothubs), green (coldhubs), yellow (non-hub hotspots), and blue (non-hub coldspots). The full set of visualizations is provided in *Supplementary Figure S5*.

Discussion

Thinking about amplitude, connectivity, hothubs, and coldhubs

In the last two decades, a new trend known as functional brain network analysis, which involves identification of critically connected positions as specific regions for a certain task or event, has been developed (Farahani et al., 2019; Medaglia, 2017; Bassett & Sporns, 2017; Lewis, 2009; O. Sporns, 2002). The new principle based on connectivity challenges the traditional paradigm that identifies critical regions by their levels of activation/amplitude. It is thus necessary to clarify whether or not a highly/heavily connected region also has a high activation level. Although there is a growing number of reports about either or both of the two aspects, few studies have considered the relationship between them. By using resting-state and finger tapping fMRI tests, Zhou et al. (2014) explored the fractional amplitudes of the lower-frequency fluctuations and the thalamic seed-based functional connectivity in persons affected by mild traumatic brain injuries. Although these researchers did not provide quantitative measurements for the amplitude–connectivity relations, their side-by-side comparison revealed co-occurring amplitude and connectivity decreases. This finding suggests that the target patients had attenuated thalamocortical networks (Zhou et al., 2014). Furthermore, based on resting-state fMRI tests, Zhang et al. (2015) defined the amplitude–connectivity coupling strength as the

correlation coefficients between the amplitude of the low-frequency fluctuation and the functional connectivity density. Compared with healthy controls, the amplitude–connectivity coupling strengths in persons having mesial temporal lobe epilepsy were found to be significantly lower in the mesial temporal structures and significantly higher in the default-mode regions. This suggests that the amplitude–connectivity uncoupling pattern can be used for differentiating patients with healthy controls. Base on a picture-naming test via MEG scanning, the present study investigated the task-state amplitude–connectivity correlation. We expanded the field by answering the following two questions.

First, do amplitude–connectivity relationships exist across scales? This question considers whether amplitude–connectivity relationships occur in different spaces and at different times. For the second aspect, we utilized a MEG naming test with a six-stages of separation (see **Figures 3, 4, and 5**) (Hassan et al., 2015). For the first aspect, we adopted island decomposition (de Nooy et al., 2018) as the thresholding method for brain graph modeling. This method establishes continuums for brain graphs and allows distributions of amplitude–connectivity patterns in the continuums to be found (see *Supplementary Figures S1, S2*).

Second, how can the most important brain regions be identified? In the amplitude dimension, the hotspots having high activity levels are responsible for the task performance. In the connectivity dimension, the highly connected hubs are pivotal to signal processing. Based on both dimensions, we classified brain regions into four categories: hothubs, non-hub hotspots, coldhubs, non-hub coldspots. If the correlation of amplitude–connectivity is significant ($p < 0.05$) and strong (with coefficients approaching 1 or -1), there should be only hothubs or coldhubs. If the correlations are non-significant or significant with weak coefficients, there should be four types of nodes in functional brain networks, and the hothubs should be the most important position, because they match both amplitude and connectivity principles.

Coupling and uncoupling amplitude–connectivity patterns in Broca and control groups

The coefficients were distributed in a similar pattern at different stages and with different graph measures (see **Figures 3, 4**, and *Supplementary Figures S1, S2*). For the Type-I deviations, the 95% confidence intervals of the two groups seldom overlapped along the island continuums. This suggests that, although both groups had amplitude–connectivity coupling relationships, their patterns were opposite. The Type-II deviations revealed the differences in the coupling and uncoupling patterns of the different groups. The controls tended to have negative values, whereas the Broca persons tended to have positive coefficients. **Figure 3** also showed that the Broca group had more coupling relationships than did the control group. For example, the t_2 and t_3 of the k -coreness, Laplace, and eigenvector had Type-II deviations with positive correlations in the

Broca group. These findings suggest that, at the object recognition (t2) and memory-access (t3) stage, the regions having high activation levels tended to be hubs (by eigenvector centrality) in core structures (by k -coreness), and they occupied critical positions (by Laplacian centrality) in the Broca aphasics. However, the interesting findings of our study were that the healthy controls had uncoupling or opposite patterns, compared with the Broca patients. This implies that the amplitude and connectivity of healthy persons are usually independent (as indicated by the uncoupling pattern) or negatively related to each other (as indicated by the coupling pattern with negative coefficients). We can thus theorize that a healthy brain follows the principle of least effort. That is, to perform a task without requesting more resources, the highly activated regions tend to run without unnecessary weak connections.

Close analysis of the coefficient distributions in **Figure 3** (and *Supplementary Figures S1*) yielded further detailed findings. Betweenness appears to be a measure that is usually uncoupled with amplitude, especially in islands having small m -values (see *Supplementary Figures S1*), suggesting that the highly activated regions did not necessarily work to transport information between other regions. The transitivity shows mixed distribution patterns for the coefficients across all naming stages. As the transitivity measures the clustering possibility of a node's first neighbors, it seems that healthy persons tended to form highly clustered structures of low activation regions during t3 to t6 in islands having large m values (see **Figure 3** and *Supplementary Figures S1*). The Broca persons considered in this study exhibited the opposite distribution (i.e., the low activation regions had lower neighborhood clustering coefficients). This suggests that, during memory access (t3), semantic processing (t4), phonological encoding (t5), and articulation (t6), the low-activation regions in the patient's brain lost their internal organizations, and their highly excited regions formed a greater number of connections among their neighbors for task performance. That is, the impaired brain recruited more local-neighbor resources to perform the same tasks (Medaglia, 2017).

The weighted degree, k -coreness, and Laplacian centrality indicated negative coefficients in the $m=776$ islands during t1 (see **Figure 3**), but they showed positive coefficients in most m -islands (see *Supplementary Figures S1*). This suggests that weakly weighted edges (indicated by the $m=776$ islands, see **Figure 3**) in the Broca group supported low activation regions while being central (by the weighted degree), core (by the k -coreness), and critical (by the Laplacian centrality). However, most edges (in m -islands other than $m=776$, see *Supplementary Figures S1*) allowed the highly activated regions to be central (by the weighted degree), core (by the k -coreness), and critical (by the Laplacian centrality). Moreover, the k -coreness and Laplacian centrality result from t2 to t5 show consistent forms of the positive coefficients (see **Figure 3**),

suggesting that most edges supported the highly activated regions while being core (by the k -coreness) and critical (by the Laplacian centrality). A similar pattern was obtained for the degree from t4 to t5, for the k -coreness and Laplacian centrality. Given the language production problem exhibited by the Broca persons, we can infer that these patients required more resources to reconstruct compensatory brain areas as task-specific regions. **Figure 4** (and *Supplementary Figure S2*) supports this conclusion, because, among the Broca persons, the highly activated regions tended to participate in more functional systems during the first three stages.

Hothubs interpretation

The hub detection method with participation coefficients should identify the optimal functional module partition scheme (Muldoon et al., 2016; van den Heuvel & Sporns, 2013; Gu et al., 2015; Medaglia, 2017). The eigenvector centralities allow the detection of hubs in the network without considering partition schemes (de Nooy et al., 2018). To avoid the controversy regarding partition schemes, we used the eigenvector centralities to self-consistently define the network hubs. As shown in **Figure 3**, the Broca-group, t1, t2, t3, and t6, had positive coefficients on the eigenvector centralities in m776-islands, suggesting that these patients tended to use highly activated regions as hubs. However, uncoupling distributions were apparent for t4 and t5, suggesting that the highly activated regions were not necessarily to be hubs in patients. In other words, the inference of hubs based on the region's activation level during the semantic processing and phonological encoding stage of the naming task was uncertain for the Broca group. Interestingly, the control-group t4 stage had a negative correlation, implying significant coldhubs at this stage.

We identified the hothubs in the averaged brain of each group. The regions in **Figure 5** were both hotspots having amplitudes exceeding the mean-plus-one standard deviation and hubs having top-level eigenvector centralities for the same number of hotspots. First, the results suggest that there were only several intersections between the two groups. That is, the patients reorganized their functional brain networks using different sets of regions as their hothubs in response to the naming task. The hothubs in **Figure 5** were mostly reported as naming specific regions (as shown in *Supplementary Table S2*). Note that some regions support cognitive functions related to naming tasks, such as visual recognition, long-term memory processing, and object configuration by the right posterior fusiform gyrus (Song, Peng, Liu, & Wang, 2019). Second, the significantly attenuated regions, such as InfOcciGyr_VenPst_R (right inferior occipital gyrus ventroposterior) in t1, and MidOcciGyr_DsoAnt_L (left middle occipital gyrus dorsal anterior) and PreCune_Sup_R (right precuneus superior) in t2, also acted as hothubs in the

Broca group. However, during the entire naming process, the Broca group used specific hothubs for which the activation levels did not differ from the control group. Third, both groups commanded more than one functional system at each stage. This suggests that naming should be a cross-modular task. Because our Broca participants were tested at least 5 months after their onset (see **Table 1**), we can infer that our observations were the results of functional reorganizations. The different hothubs and functional systems in each group (as detailed in **Figure 5**) suggest that there were both intrasystem and intersystem reorganizations in the Broca group.

Network visualizations and coldhubs exploration

For more detailed inspections of these reorganizations, we visualized each graph by categorizing the refined 776 regions into four types (as shown in **Figure 6** and *Supplementary Figure S5*). **Figure 6** is an example of amplitude and linking-strength distributions in t4. Coldhubs are always present in each graph. For example, the left SupFrtGyr_Pst (superior frontal gyrus posterior, see **Fig.6 arrow a**) and MidTempGyr_Mid (middle temporal gyrus middle, see **Fig.6 arrow b**) are coldhubs occupying critical positions on the dorsal and ventral stream at the semantic processing stage. These coldhubs cannot be visualized by the traditional imaging strategy that depends on the scout activation level. Focusing on the linking-strength panels could reveal that the coldhubs (green nodes) exhibit a different functional brain network landscape. From these findings, a partial answer to the question raised by Heuvel and Sporns on whether brain hubs are potential hot spots with clinical meaning could be derived (van den Heuvel & Sporns, 2013). Network hubs are possible but not necessarily bound to be hot spots. Patients and their healthy controls differed both in the hothubs and in the coldhubs. The dark functional networks formed by coldhubs deserve more considerations in future studies.

Methodological considerations, limitations, and clinical implications

Our study has several limitations. First, the connectivity modeling in MEG has spatial leakage problems (J. Matias Palva et al., 2018; Colclough et al., 2016; Brookes, Woolrich, & Barnes, 2012). PLV is a method lacking leakage correction (Colclough et al., 2016). Palva et al. recommended that researchers perform the full source-space interaction mapping rather than applying a seed-based approach (J. Matias Palva et al., 2018). We utilized the connectivity strategy to interpret undirected graphs based on PLVs across the whole cerebral cortex. Hassan et al. (2015) previously used such graphs for studying picture-naming. They constructed an atlas with 1000 scouts covering the whole cortex, calculated PLVs based on the source space estimated by the WMNE method, and normalized PLVs to reduce artefactual inflated connectivity. We constructed 776 scouts covering the whole cortex, calculated PLVs based on

WMNE, and also normalized PLVs as connection weights. According to Hincapié et al., if the interacting sources were extended patches having several dipoles in them, the minimum-norm estimation would provides better connectivity estimation than would the beamformer (Hincapié et al., 2017). We know that these considerations might not fully resolve the controversy about using PLV. This is an ongoing issue. Rizkallah et al. reported that PLV metrics of MEGs were significantly correlated with fMRI networks compared with other zero-lag corrected methods (Rizkallah, Amoud, Fraschini, Wendling, & Hassan, 2020). Our report encourages us to explore more types of functional and effective connectivity in future works. For example, the phase-transfer entropy will establish directed graphs for detailed inspections of information flows in the brain (Engels et al., 2017).

Second, the estimated source values of the WMNE tended to be reduced with increasing depths, varying significantly between subjects. The Brainstorm's guides recommended using the current density map for computing connectivity measures. Although the coupling patterns explored by our study were based on within-subject analyses, we still reported findings based on the raw current density values in the unit of picoamperes. We also projected all source spaces into the same template to reduce the influences of inter-individual differences.

Third, we are aware of our small participant sample and the inconsistencies of stroke victims. One of the participants (B5) was significantly younger than the others. Although this is a possible confounding factor, the maximum variation strategy provides another view (Patton, 2014). If there any patterns were to emerge, despite the great variation, the patterns would have value in capturing the essential impacts of a program. Therefore, the amplitude–connectivity correlation patterns found in this study made sense for our original hypothesis. On the other hand, the effects of individuals were adjusted via partial correlation analysis. That was, we treated the individuals as the third variable when calculating the amplitude–connectivity correlation coefficients.

Fourth, the stroked structure should be considered in the study. There were brain volumes with encephalomalacia that could influence the results of source reconstruction. This is a technical problem without a satisfactory solution in the head-modeling and brain parcellation. The stroked-out areas remained part of the source space. Therefore, the results of stroke persons were estimates based on virtual structures of the brain. Nevertheless, the control group should not be influenced by this problem, and results from them should make sense for our hypothesis. Besides, the amplitude–connectivity relationships between groups remained unchanged after removing the stroked left hemisphere in both groups (see *Supplementary Figures S6 and S7*). Moreover, clinical applications of transcranial brain stimulation (e.g., repetitive transcranial

magnetic stimulation) usually inject electric currents into the brain by inversely assuming the source space of stimulation (Biou et al., 2019; Norise & Hamilton, 2017; Coslett, 2016). With the rapid expansion of non-invasive brain stimulation technology, the effective target region location is an issue strongly associated with clinical application. Therapists should decide to use one of two opposite strategies to execute stimulation (viz., to excite or inhibit a target position) (Biou et al., 2019; Norise & Hamilton, 2017; Polania, Nitsche, & Ruff, 2018). Essentially, their decisions related to excitatory or inhibitory stimulation protocols are related to the hot or cold spots. The amplitude–connectivity correlation study reported herein presents a new perspective on this question by revealing the dark functional networks with coldhubs in the reconstructed source space. The effects of brain stimulation on the cold and hot hubs may differ and require more study. Further study should include more participants to confirm the cross-scale deviation patterns of the amplitude–connectivity relationships.

Apart from the perspective of brain stimulation, speech-language therapy is another field related to our findings. Picture-naming is a widely used therapy task in speech-language therapy. However, various variables can influence the outcomes of linguistic therapy, including but not limited to semantic and phonological factors in picture-naming (Nakagawa, Sano, Funayama, & Kato, 2019; Shrubsole, Worrall, Power, & O’Connor, 2017). One future direction is to find links between graph measures and behavioral performances (Meier, Johnson, & Kiran, 2018; Meier, Kapse, & Kiran, 2016; J. M. Palva, Monto, Kulashekhar, & Palva, 2010). Another future work is to find associations between variables embedded in stimuli, such as semantic components based on semantic feature norms (Feng LIN, 2015), and graph measures of hothubs and coldhubs. Then, the speech-language pathologist would be able to arrange brain modifying stimuli during therapy.

Conclusions

In this study, we investigated the activation–connection correlations for the performance of naming tasks by persons having post-stroke aphasia compared with healthy subjects. Although this study observed a small sample of participants with regards to a simple naming paradigm, it expanded our knowledge of hothubs by integrating both the activation and connection. The results reveal that the examined patients utilized different activation–connection coupling patterns and different sets of hothubs as healthy participants to perform the same task, thereby functionally reorganizing their brains. The findings also indicate that there were hubs with low activations in functional brain networks. Thus, dark functional networks must be considered in functional brain-imaging studies. The operational concepts of “hothubs” and “dark functional

networks” will promote further development of target-selection approaches to therapeutic brain stimulation.

Acknowledgments

We appreciate Dr. Chun FENG from the University of Nebraska Medical Center, for her kind editorial assistance with our manuscript.

Data Availability

The following information was supplied regarding data availability:

Zenodo database: Functional Brain Networks of Picture Naming in Broca's Aphasia and Healthy Controls. ID: 3831117. <https://doi.org/10.5281/zenodo.3831117>

References

- Baillet, S. (2017). Magnetoencephalography for brain electrophysiology and imaging. *Nature Neuroscience*, 20(3), 327–339. doi: 10.1038/nn.4504
- Barrat, A., Barthelemy, M., Pastor-Satorras, R., & Vespignani, A. (2004). The architecture of complex weighted networks. *Proceedings of the National Academy of Sciences*, 101(11), 3747–3752. doi: 10.1073/pnas.0400087101
- Bassett, D. S., Khambhati, A. N., & Grafton, S. T. (2017). Emerging frontiers of neuroengineering: A network science of brain connectivity. *Annual Review of Biomedical Engineering*, 19, 327–352. doi: 10.1146/annurev-bioeng-071516-044511
- Bassett, D. S., & Sporns, O. (2017). Network neuroscience. *Nature Neuroscience*, 20(3), 353–364. doi: 10.1038/nn.4502
- Biou, E., Cassoudeulle, H., Cogne, M., Sibon, I., De Gabory, I., Dehail, P., ... Glize, B. (2019). Transcranial direct current stimulation in post-stroke aphasia rehabilitation: A systematic review. *Annals of Physical and Rehabilitation Medicine*, 62(2), 104–121. doi: 10.1016/j.rehab.2019.01.003
- Biswal, B. B. (2012). Resting state fMRI: A personal history. *NeuroImage*, 62(2), 938–944. doi: 10.1016/j.neuroimage.2012.01.090
- Brookes, M. J., Woolrich, M. W., & Barnes, G. R. (2012). Measuring functional connectivity in MEG: A multivariate approach insensitive to linear source leakage. *NeuroImage*, 63(2), 910–920. doi: 10.1016/j.neuroimage.2012.03.048
- Calin-Jageman, R. J., & Cumming, G. (2019). Estimation for Better Inference in Neuroscience. *Eneuro*, 6(4), ENEURO.0205-19.2019. doi: 10.1523/ENEURO.0205-19.2019

- Colclough, G. L., Woolrich, M. W., Tewarie, P. K., Brookes, M. J., Quinn, A. J., & Smith, S. M. (2016). How reliable are MEG resting-state connectivity metrics? *Neuroimage*, 138, 284–293. doi: 10.1016/j.neuroimage.2016.05.070
- Coslett, H. B. (2016). Noninvasive brain stimulation in aphasia therapy: Lessons from TMS and tDCS. In G. Hickok & S. L. Small (Eds.), *Neurobiology of Language* (pp. 1035–1054). Retrieved from <https://doi.org/10.1016/B978-0-12-407794-2.00083-3>
- Csardi, G., & Nepusz, T. (2006). The igraph software package for complex network research. *InterJournal, Complex Systems*, 1695(5), 1–9.
- Daffertshofer, A., & van Wijk, B. C. M. (2011). On the Influence of Amplitude on the Connectivity between Phases. *Frontiers in Neuroinformatics*, 5. doi: 10.3389/fninf.2011.00006
- de Nooy, W., Mrvar, A., & Batagelj, V. (2018). *Exploratory social network analysis with Pajek* (3rd ed.). New York: Cambridge University Press.
- De Vico Fallani, F., Richiardi, J., Chavez, M., & Achard, S. (2014). Graph analysis of functional brain networks: Practical issues in translational neuroscience. *Philosophical Transactions of the Royal Society B: Biological Sciences*, 369(1653), 20130521. doi: 10.1098/rstb.2013.0521
- Dinga, S., Wu, D., Huang, S., Wu, C., Wang, X., Shi, J., ... Xiang, J. (2018). Neuromagnetic correlates of audiovisual word processing in the developing brain. *International Journal of Psychophysiology*, 128, 7–21. doi: 10.1016/j.ijpsycho.2018.03.016
- Ellis, A. W., Burani, C., Izura, C., Bromiley, A., & Venneri, A. (2006). Traces of vocabulary acquisition in the brain: Evidence from covert object naming. *Neuroimage*, 33(3), 958–968. doi: 10.1016/j.neuroimage.2006.07.040
- Engels, M. M. A., Yu, M., Stam, C. J., Gouw, A. A., van der Flier, W. M., Scheltens, Ph., ... Hillebrand, A. (2017). Directional information flow in patients with Alzheimer’s disease. A source-space resting-state MEG study. *NeuroImage: Clinical*, 15, 673–681. doi: 10.1016/j.nicl.2017.06.025
- Farahani, F. V., Karwowski, W., & Lighthall, N. R. (2019). Application of graph theory for identifying connectivity patterns in human brain networks: A systematic review. *Frontiers in Neuroscience*, 13. doi: 10.3389/fnins.2019.00585
- Feng LIN. (2015). *A Speech-Language Therapy Oriented Strategy to Analyze Chinese Lexical-Semantic Representation* (Doctoral dissertation). Nanjing Normal University, Nanjing.
- Friston, K. J. (2011). Functional and effective connectivity: A review. *Brain Connectivity*, 1(1), 13–36. doi: 10.1089/brain.2011.0008

- Gu, S., Satterthwaite, T. D., Medaglia, J. D., Yang, M., Gur, R. E., Gur, R. C., & Bassett, D. S. (2015). Emergence of system roles in normative neurodevelopment. *Proceedings of the National Academy of Sciences*, 112(44), 13681–13686. doi: 10.1073/pnas.1502829112
- Hassan, M., Benquet, P., Biraben, A., Berrou, C., Dufor, O., & Wendling, F. (2015). Dynamic reorganization of functional brain networks during picture naming. *Cortex*, 73, 276–288. doi: 10.1016/J.CORTEX.2015.08.019
- Hassan, M., & Wendling, F. (2018). Electroencephalography source connectivity: Aiming for high resolution of brain networks in time and space. *IEEE Signal Processing Magazine*, 35(3), 81–96. doi: 10.1109/MSP.2017.2777518
- Hincapié, A.-S., Kujala, J., Mattout, J., Pascarella, A., Daligault, S., Delpuech, C., ... Jerbi, K. (2017). The impact of MEG source reconstruction method on source-space connectivity estimation: A comparison between minimum-norm solution and beamforming. *NeuroImage*, 156, 29–42. doi: 10.1016/J.NEUROIMAGE.2017.04.038
- Joshi, A. A., Choi, S., Sonkar, G., Chong, M., Gonzalez-Martinez, J., Nair, D., ... Leahy, R. M. (2017). A whole brain atlas with sub-parcellation of cortical gyri using resting fMRI. In M. A. Styner & E. D. Angelini (Eds.), *Proceedings of SPIE, Medical Imaging: Image Processing* (Vol. 10133, pp. 101330O – 9). doi: 10.1117/12.2254681
- Kent, G. H., & Rosanoff, A. J. (1910). A study of association in insanity. *American Journal of Psychiatry*, 67(1), 37–96. doi: 10.1176/ajp.67.1.37
- Laganaro, M., Morand, S., Schwitter, V., Zimmermann, C., & Schnider, A. (2008). Normalisation and increase of abnormal ERP patterns accompany recovery from aphasia in the post-acute stage. *Neuropsychologia*, 46(8), 2265–2273. doi: 10.1016/j.neuropsychologia.2008.02.013
- Levelt, W. J., Praamstra, P., Meyer, A. S., Helenius, P., & Salmelin, R. (1998). An MEG study of picture naming. *Journal of Cognitive Neuroscience*, 10(5), 553–567. doi: 10.1162/089892998562960
- Lewis, T. G. (2009). *Network science: Theory and practice*. Hoboken, New Jersey,USA: John Wiley & Sons, Inc.
- Medaglia, J. D. (2017). Functional neuroimaging in traumatic brain injury: From nodes to networks. *Frontiers in Neurology*, 8, 407. doi: 10.3389/fneur.2017.00407
- Meier, E. L., Johnson, J. P., & Kiran, S. (2018). Left frontotemporal effective connectivity during semantic feature judgments in patients with chronic aphasia and age-matched healthy controls. *Cortex*, 108, 173–192. doi: 10.1016/j.cortex.2018.08.006

- Meier, E. L., Kapse, K. J., & Kiran, S. (2016). The Relationship between Frontotemporal Effective Connectivity during Picture Naming, Behavior, and Preserved Cortical Tissue in Chronic Aphasia. *Frontiers in Human Neuroscience*, 10. doi: 10.3389/fnhum.2016.00109
- Michel, C. M., & Brunet, D. (2019). EEG source imaging: A practical review of the analysis steps. *Frontiers in Neurology*, 10. doi: 10.3389/fneur.2019.00325
- Mrvar, A., & Batagelj, V. (2016). Analysis and visualization of large networks with program package Pajek. *Complex Adaptive Systems Modeling*, 4, 6. doi: 10.1186/s40294-016-0017-8
- Muldoon, S. F., Pasqualetti, F., Gu, S., Cieslak, M., Grafton, S. T., Vettel, J. M., & Bassett, D. S. (2016). Stimulation-based control of dynamic brain networks. *PLoS Computational Biology*, 12(9), e1005076. doi: 10.1371/journal.pcbi.1005076
- Nakagawa, Y., Sano, Y., Funayama, M., & Kato, M. (2019). Prognostic factors for long-term improvement from stroke-related aphasia with adequate linguistic rehabilitation. *Neurological Sciences*, 40(10), 2141–2146. doi: 10.1007/s10072-019-03956-7
- Norise, C., & Hamilton, R. H. (2017). Non-invasive brain stimulation in the treatment of post-stroke and neurodegenerative aphasia: Parallels, differences, and lessons learned. *Frontiers in Human Neuroscience*, 10, 675. doi: 10.3389/fnhum.2016.00675
- Palva, J. M., Monto, S., Kulashekhar, S., & Palva, S. (2010). Neuronal synchrony reveals working memory networks and predicts individual memory capacity. *Proceedings of the National Academy of Sciences*, 107(16), 7580–7585. doi: 10.1073/pnas.0913113107
- Palva, J. Matias, Wang, S. H., Palva, S., Zhigalov, A., Monto, S., Brookes, M. J., ... Jerbi, K. (2018). Ghost interactions in MEG/EEG source space: A note of caution on inter-areal coupling measures. *NeuroImage*, 173, 632–643. doi: 10.1016/j.neuroimage.2018.02.032
- Patton, M. Q. (2014). *Qualitative research & evaluation methods: Integrating theory and practice* (4th ed.). USA: SAGE Publications.
- Pavlopoulos, G. A., Paez-Espino, D., Kyrpides, N. C., & Iliopoulos, I. (2017). Empirical comparison of visualization tools for larger-scale network analysis. *Advances in Bioinformatics*, 2017, 1278932. doi: 10.1155/2017/1278932
- Polania, R., Nitsche, M. A., & Ruff, C. C. (2018). Studying and modifying brain function with non-invasive brain stimulation. *Nature Neuroscience*, 21(2), 174–187. doi: 10.1038/s41593-017-0054-4
- Qi, X., Duval, R. D., Christensen, K., Fuller, E., Spahiu, A., Wu, Q., ... Zhang, C. (2013). Terrorist networks, network energy and node removal: A new measure of centrality based on laplacian energy. *Social Networking*, 02(01), 19–31. doi: 10.4236/sn.2013.21003

- 731 Raichle, M. E. (2006). The brain's dark energy. *Science*, 314(5803), 1249–1250. doi:
732 10.1126/science. 1134405
- 733 Revelle, W. (2019). psych: Procedures for personality and psychological research (Version
734 1.8.12) [R]. Retrieved from <https://CRAN.R-project.org/package=psych>
- 735 Rizkallah, J., Amoud, H., Fraschini, M., Wendling, F., & Hassan, M. (2020). Exploring the
736 Correlation Between M/EEG Source–Space and fMRI Networks at Rest. *Brain*
737 *Topography*, 33(2), 151–160. doi: 10.1007/s10548-020-00753-w
- 738 Rubinov, M., & Sporns, O. (2010). Complex network measures of brain connectivity: Uses and
739 interpretations. *NeuroImage*, 52(3), 1059–1069. doi: 10.1016/j.neuroimage.2009.10.003
- 740 Salmelin, R., Hari, R., Lounasmaa, O. V., & Sams, M. (1994). Dynamics of brain activation
741 during picture naming. *Nature*, 368(6470), 463–465. doi: 10.1038/368463a0
- 742 Shrubsole, K., Worrall, L., Power, E., & O'Connor, D. A. (2017). Recommendations for post-
743 stroke aphasia rehabilitation: An updated systematic review and evaluation of clinical
744 practice guidelines. *Aphasiology*, 31(1), 1–24. doi: 10.1080/02687038.2016.1143083
- 745 Song, L., Peng, Q., Liu, S., & Wang, J. (2019). Changed hub and functional connectivity patterns
746 of the posterior fusiform gyrus in chess experts. *Brain Imaging and Behavior*. doi:
747 10.1007/s11682-018-0020-0
- 748 Sporns, O. (2002). Network analysis, complexity, and brain function. *Complexity*, 8(1), 56–60.
749 doi: 10.1002/cplx.10047
- 750 Sporns, Olaf. (2016). *Networks of the Brain*. S.I.: The MIT Press.
- 751 Tadel, F., Baillet, S., Mosher, J. C., Pantazis, D., & Leahy, R. M. (2011). Brainstorm: A user-
752 friendly application for MEG/EEG analysis. *Computational Intelligence and Neuroscience*,
753 2011, 879716. doi: 10.1155/2011/879716
- 754 Tadel, F., Bock, E., Niso, G., Mosher, J. C., Cousineau, M., Pantazis, D., ... Baillet, S. (2019).
755 MEG/EEG group analysis with Brainstorm. *Frontiers in Neuroscience*, 13, 76. doi:
756 10.3389/fnins.2019.00076
- 757 van den Heuvel, M. P., & Sporns, O. (2013). Network hubs in the human brain. *Trends in*
758 *Cognitive Sciences*, 17(12), 683–696. doi: 10.1016/j.tics.2013.09.012
- 759 van Eck, N., & Waltman, L. (2009). Software survey: VOSviewer, a computer program for
760 bibliometric mapping. *Scientometrics*, 84(2), 523–538. doi: 10.1007/s11192-009-0146-3
- 761 Vargas, E. R., & Wahl, L. M. (2014). The gateway coefficient: A novel metric for identifying
762 critical connections in modular networks. *The European Physical Journal B*, 87, 161. doi:
763 10.1140/epjb/e2014-40800-7

- Wang, H., Bing, W., & Hou, Y. (2010). A comparison study on word association between English native speakers and Chinese English learners. *Canadian Social Science*, 6(6), 45–60.
- Watson, C. G. (2019). brainGraph: Graph theory analysis of brain MRI data (Version 2.2.0.) [R]. Retrieved from <https://github.com/cwatson/brainGraph>
- Xiang, J., Wilson, D., Otsubo, H., Ishii, R., & Chuang, S. (2001). Neuromagnetic spectral distribution of implicit processing of words. *Neuroreport*, 12(18), 3923–3927. doi: 10.1097/00001756-200112210-00014
- Youssofzadeh, V., & Babajani-Feremi, A. (2019). Mapping critical hubs of receptive and expressive language using MEG: A comparison against fMRI. *NeuroImage*, 201, 116029. doi: 10.1016/j.neuroimage.2019.116029
- Zhang, Z., Xu, Q., Liao, W., Wang, Z., Li, Q., Yang, F., ... Lu, G. (2015). Pathological uncoupling between amplitude and connectivity of brain fluctuations in epilepsy. *Human Brain Mapping*, 36(7), 2756–2766. doi: 10.1002/hbm.22805
- Zhou, Y., Lui, Y. W., Zuo, X.-N., Milham, M. P., Reaume, J., Grossman, R. I., & Ge, Y. (2014). Characterization of thalamo-cortical association using amplitude and connectivity of functional MRI in mild traumatic brain injury. *Journal of Magnetic Resonance Imaging*, 39(6), 1558–1568. doi: 10.1002/jmri.24310

Figure 1

Experiment paradigm

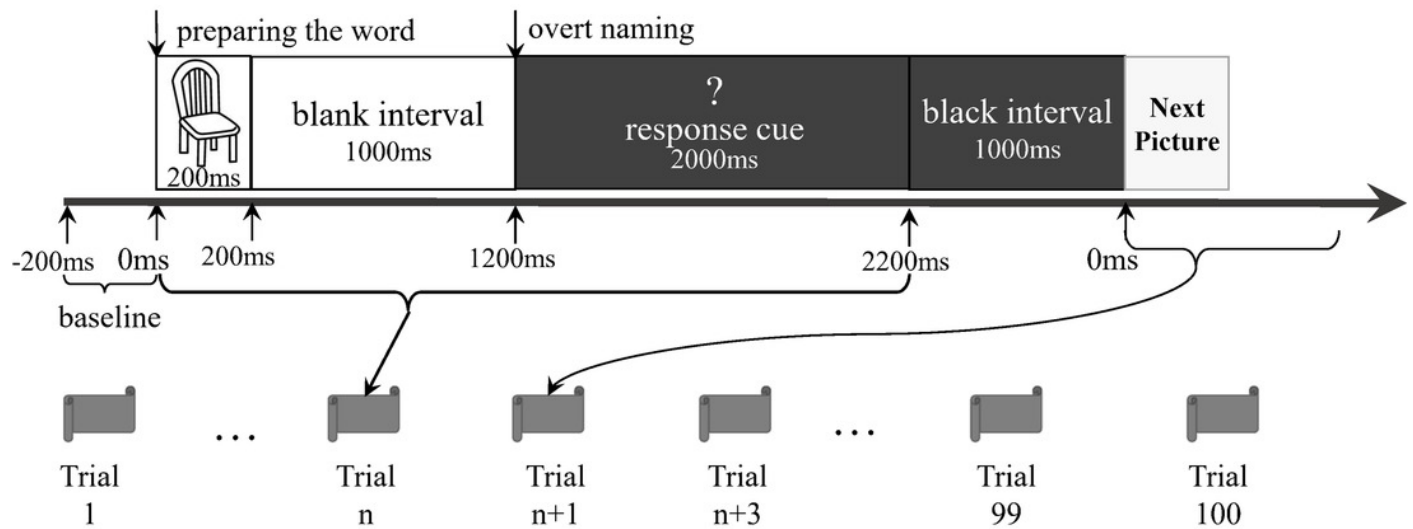


Figure 2

Data processing workflow

The dashed curved arrow denotes that the final reported m776 and m388 islands are selected from a series of m values by interpreting the *Supplementary Figures S1, S2*. MEG: magnetoencephalography; MRI: magnetic resonance imaging.

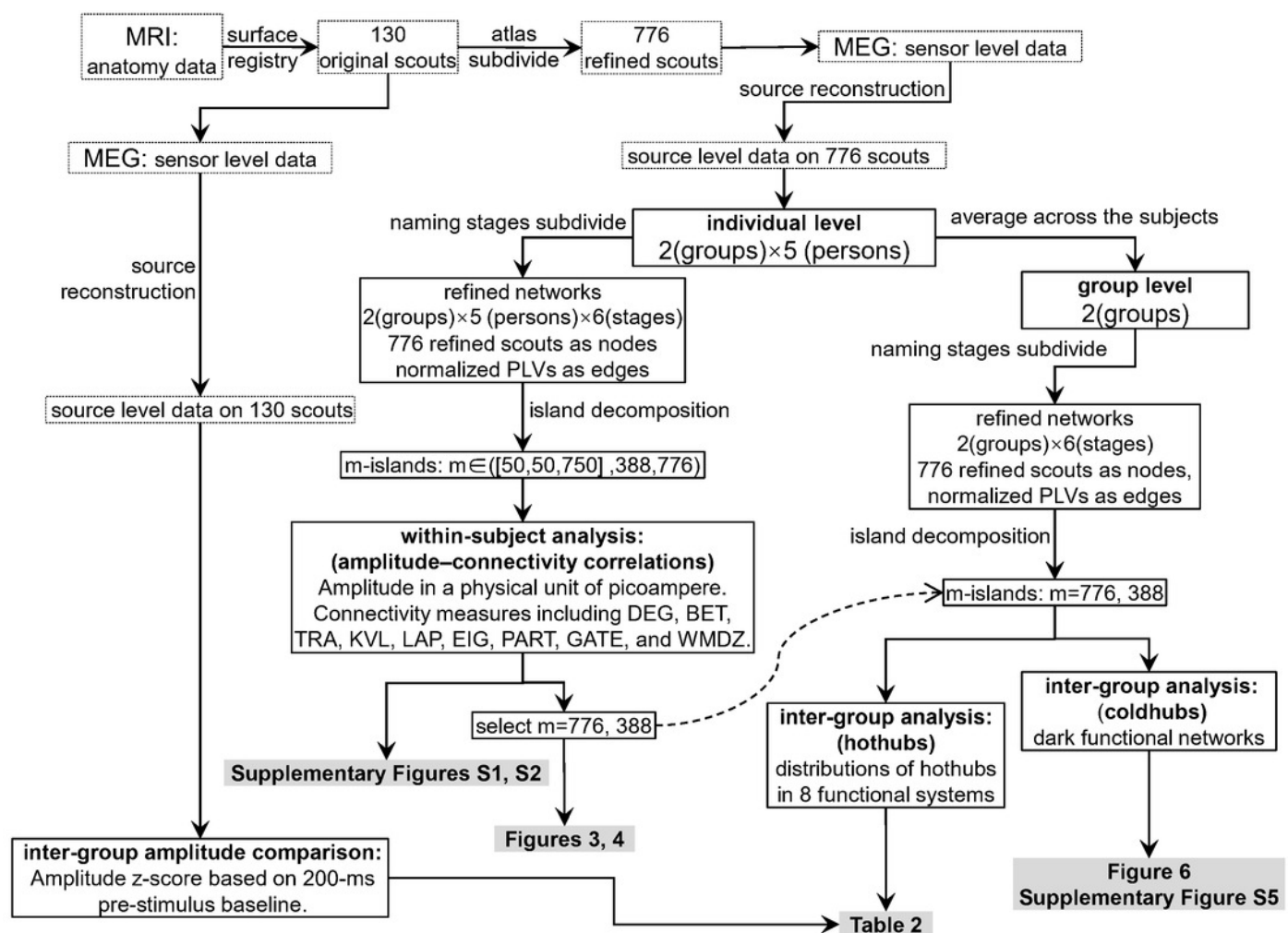


Figure 3

Relations between activations (picoampere) and module-independent graph measures in m776-islands

Activations are the estimated electric densities (in a physical unit of picoampere) in the source space. The partial Pearson coefficients between the activations and graph measures are calculated for m776-islands at different stages. The significant coefficients ($p < 0.05$) are marked with asterisks. The 95% confidence intervals having significant coefficients are marked by transparent colored bars. DEG: weighted degree; BET: weighted betweenness; TRA: weighted transitivity; KVL: k-value of coreness; LAP: Laplacian centrality; EIG: eigenvector centrality; t1: 0–119 ms, visual feature extraction; t2: 120–150 ms, object recognition; t3: 151–190 ms, memory access; t4: 191–320 ms, semantic processing; t5: 321–480 ms, phonological encoding; t6: 481–535 ms, articulation. A positive coefficient marked with an asterisk denotes that strongly activated brain regions are more likely to be highly connected hubs. A negative coefficient marked with an asterisk suggests that highly connected hubs are more likely to be with weak intensities of activation. The separation of the confidence intervals having opposite values of coefficients infers that the two groups have significantly different amplitude–connectivity relationships. One significant correlation having another nonsignificant correlation also implies that there are interconditional differences of amplitude–connectivity relationships.

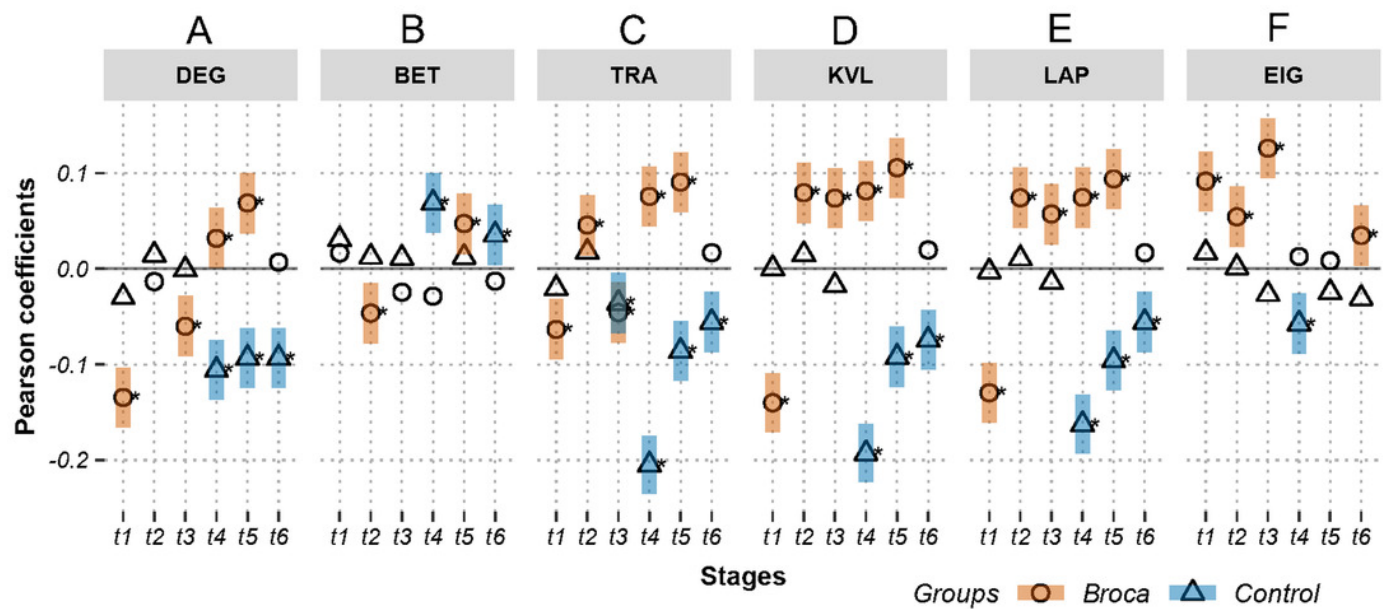


Figure 4

Relations between activations (picoampere) and module-dependent graph measures in m388-islands

Activations are the estimated electric densities (in a physical unit of picoampere) in the source space. The partial Pearson coefficients between the activations and graph measures are calculated for m388-islands at different stages. The significant coefficients ($p < 0.05$) are marked with asterisks. The 95% confidence intervals having significant coefficients are marked by transparent colored bars. PART: participation coefficient; GATE: gateway coefficient; WMDZ: within module degree z-score; t1: 0–119 ms, visual feature extraction; t2: 120–150 ms, object recognition; t3: 151–190 ms, memory access; t4: 191–320 ms, semantic processing; t5: 321–480 ms, phonological encoding; t6: 481–535 ms, articulation. A positive coefficient marked with an asterisk denotes that strongly activated brain regions are more likely to be highly connected hubs. A negative coefficient marked with an asterisk suggests that highly connected hubs are more likely to be with weak intensities of activation. The separation of the confidence intervals with opposite values of coefficients infers that the two groups have significantly different amplitude–connectivity relationships. One significant correlation with another nonsignificant correlation also implies that there are interconditional differences of amplitude–connectivity relationships.

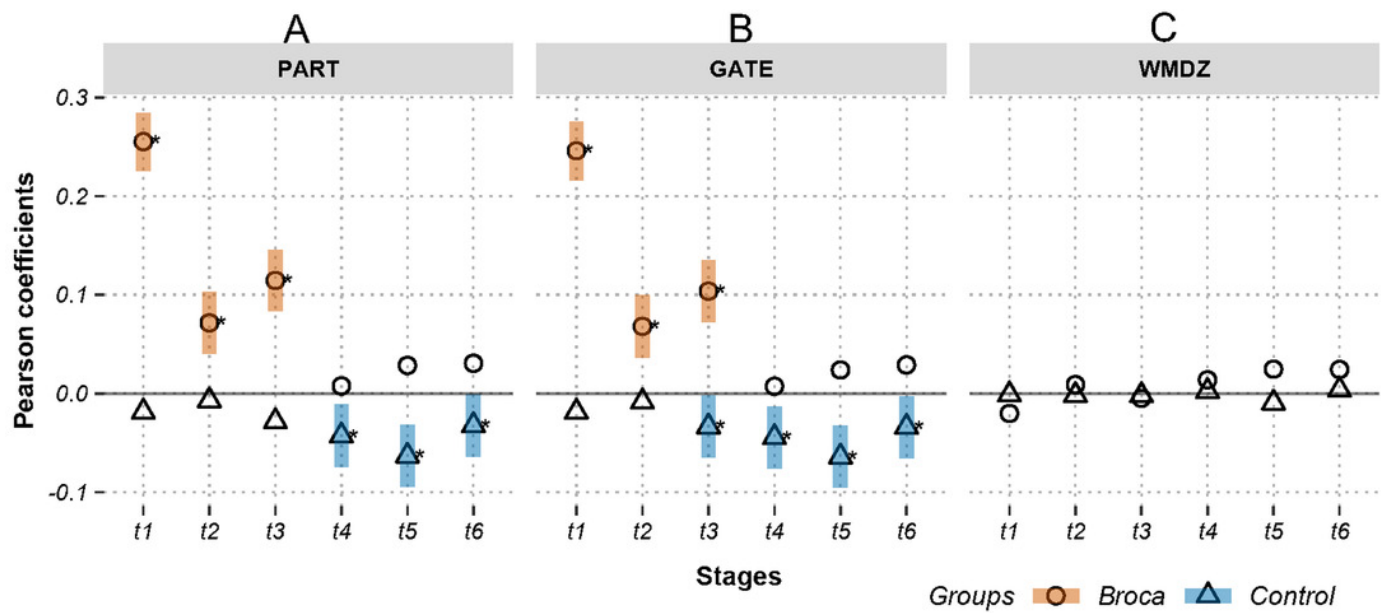


Figure 5

Hothubs in m776-islands

a: Significantly lower z-scores for amplitudes of Broca group than those of the control group (permutation t-test, 1,000 randomizations). b: Significantly higher z-scores for amplitudes of control group than those of Broca group (permutation t-test, 1,000 randomizations). t1: InfOcciGyr_VenPst_R ($p=0.016$), SupPariGyr_Pst_R ($p=0.008$), PreCune_Sup_L ($p=0.02$). t2: PreCune_Sup_R ($p=0.046$), MidOcciGyr_DsoAnt_L ($p=0.004$). t3: SupPariGyr_Ant_R ($p=0.016$), PreCune_Sup_L ($p=0.024$), PreCune_Sup_R ($p=0.017$), SupFrtGyr_Ant_L ($p=0.039$). Colors for functional modules: Pink: attention; orange: auditory; yellow: cinguloopercular; blue: frontoparietal; green: medial default mode; grey: motor and somatosensory; lilac: ventral temporal association; white: visual.

	A	B	C	D	E	F
	t1	t2	t3	t4	t5	t6
Broca	SupTepGyr-Pst-L	ParsOrbitalis-R	LatObtFrtGyr-Pst-L	SupPariGyr-Pst-L	LatObtFrtGyr-Pst-R	LatObtFrtGyr-Pst-L&R
	AnguGyr-Pst-R	PreCune-Sup-R ^a	SupPariGyr-Pst-L	AnguGyr-Mid-L	AnguGyr-Mid-R	SupTepGyr-Pst-L
	Insula-Ant-R	PreCentGyr-Sup-L	TsvTepGyr-L	PreCune-Inf-R	GyrRectus-L&R	ParsOpcu-Inf-R
	MidOcciGyr-VenAnt-L	Cune-Pst-L&R	ParsOrbitalis-R	PostCentGyr-Inf-L	Insula-Ant-L	AnguGyr-Ant-L
	Cune-Pst-R	LingualGyr-Ant-R	GyrRectus-R	MidTepGyr-DsoPst-L	MidObtFrtGyr-L	AnguGyr-Mid-L
	InfOcciGyr-VenPst-R ^a	MidOcciGyr-DsoAnt-L ^a	MidObtFrtGyr-R	Cune-Pst-L	ParsTriagu-Mid-L	Insula-Ant-L
	LingualGyr-Pst-R	MidOcciGyr-VenAnt-L	Cune-Ant-R	InfOcciGyr-Ant-R	TsvFrtGyr-Lat-R	ParsTriagu-Mid-L
	SupOcciGyr-Inf-L	SupOcciGyr-Sup-L	InfOcciGyr-Ant-R	InfOcciGyr-DsoPst-L	PstObtFrtGyr-L	PreCentGyr-Inf-L
	SupOcciGyr-Sup-R		InfOcciGyr-VenPst-R	LingualGyr-Ant-R	MidTepGyr-DsoPst-L	MidTepGyr-DsoPst-L
			LingualGyr-Ant-R	LingualGyr-Pst-R	MidTepGyr-VenPst-L	MidTepGyr-VenPst-L
			MidOcciGyr-DsoAnt-L	MidOcciGyr-Pst-R	LingualGyr-Ant-R	InfOcciGyr-Ant-L
			MidOcciGyr-VenAnt-L	MidOcciGyr-VenAnt-L	MidOcciGyr-DsoAnt-L	LingualGyr-Pst-R
						MidOcciGyr-DsoAnt-L
						MidOcciGyr-VenAnt-L
Control	LatObtFrtGyr-Pst-L	MidFrtGyr-Ant-R	LatObtFrtGyr-Ant-R	SupTepGyr-Ant-L	MidFrtGyr-Ant-R	CingGyr-Ant-R
	SupPariGyr-Pst-R ^b	AnguGyr-Pst-R	SupPariGyr-Ant-R ^b	TsvTepGyr-L	FusiGyr-Pst-R	SprmarGyr-Pst-R
	MidFrtGyr-Ant-R	Cune-Ant-L	SupPariGyr-Pst-R	MidFrtGyr-Ant-R	InfTepGyr-Ant-L	AntObtFrtGyr-R
	AntObtFrtGyr-R	Cune-Pst-R	ParsOpcu-Sup-L	AnguGyr-Ant-L	InfOcciGyr-Ant-L	ParsTriagu-Ant-R
	TsvFrtGyr-Msl-R	SupOcciGyr-Inf-R	AnguGyr-Mid-L	AnguGyr-Pst-L&R	SupOcciGyr-Sup-L	SupFrtGyr-Pst-R
	PstObtFrtGyr-L	SupOcciGyr-Sup-R	MidFrtGyr-Pst-R	AntObtFrtGyr-R		PreCentGyr-Inf-R
	TepPole-L		PstObtFrtGyr-R	MidObtFrtGyr-R		FusiGyr-Pst-R
	Cune-Pst-L		CingGyr-Mid-L	ParsTriagu-Ant-L		MidTepGyr-Ant-R
	MidOcciGyr-VenAnt-R		PreCune-Sup-L&R ^b	ParsTriagu-Pst-L		
	SupOcciGyr-Sup-R		SupFrtGyr-Ant-L ^b	TsvFrtGyr-Lat-R ^b		
			PreCune-Inf-L	SubcallosalGyr-R		
			InfTepGyr-Mid-R	PostCentGyr-Sup-L		
			MidTepGyr-Ant-L	SupOcciGyr-Sup-R		
			Cune-Ant-L			
Intersection	PreCune-Sup-L ^b	SupPariGyr-Pst-R	AnguGyr-Pst-R	MidOcciGyr-DsoAnt-L	LatObtFrtGyr-Ant-R	
	InfOcciGyr-VenPst-L	InfOcciGyr-DsoPst-L			MidOcciGyr-VenAnt-L	
	MidOcciGyr-Pst-R					

attention
auditory
cinguloopercular
frontoparietal
medial default mode
motor and somatosensory
ventral temporal association
visual

Figure 6

Sample amplitude and linking strength distributions in t4

Hotspots are identified based on their amplitudes that exceeded the mean-plus-one standard deviation. Hubs are identified based on their eigenvector centralities as defined in Pajek, with the same number of hotspots at each stage. For each viewpoint, node areas on the left panel are in proportion to the z-scores of their amplitudes, whereas those on the right panel are in proportion to the total linking strengths (i.e., weighted degrees). Arrow a: Left SupFrtGyr_Pst (left superior frontal gyrus posterior). Arrow b: Left MidTempGyr_Mid (left middle temporal gyrus middle). The top-weighted 100 edges are plotted, and the edges are colored according to their terminals. There are four node types: hothubs (red), coldhubs (green), non-hub hotspots (yellow), and non-hub coldspots (blue). The t4 is the semantic processing window of 191–320 ms. The amplitude weighted layouts (left panels in each viewpoint), are remarkably different from the linking strength weighted layouts (right panels in each viewpoint), suggesting that it is necessary to reconsider the role of coldhubs in functioning brain.

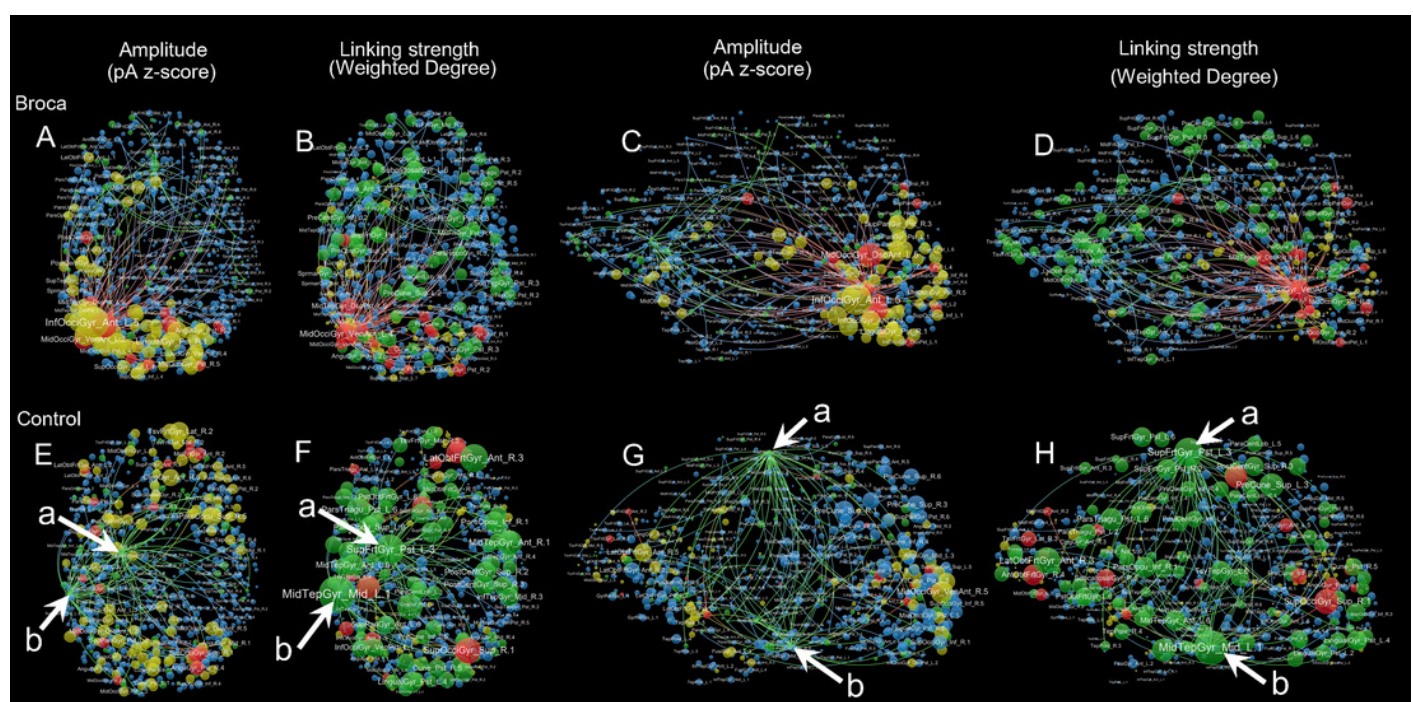


Table 1(on next page)

Demographic characteristics

AQ: aphasia quotient; B: persons with Broca’s aphasia; C: control subjects; F: frontal lobe; T: temporal lobe; P: parietal lobe; O: occipital lobe; WAB: Western Aphasia Battery. T-tests between control group and Broca’s aphasics with *P=0.30; **P=0.24; ***P=0.00092.

1 **Table 1: Demographic characteristics.**

Subjects	B1	B2	B3	B4	B5	C1	C2	C3	C4	C5
Gender (Male/Female)	Male	Male	Male	Male	Male	Female	Male	Male	Male	Male
Handedness (R/L)	R	R	R	R	R	R	R	R	R	R
Age at onset (years)*	71	50	48	55	19	68	55	55	54	70
Education duration (years)**	7	10	10	16	9	8	8	9	12	9
Time after onset (months)	8	5	5	42.7	9.4	-	-	-	-	-
Stroke type	hemorrhage	hemorrhage	infarction	hemorrhage	infarction	-	-	-	-	-
Lesion locations	left (F, T, P, O)	left (basal ganglia)	left (F, T, P)	left (basal ganglia)	left (F, T, P)	-	-	-	-	-
WAB AQ***	31.4	64.6	43.8	53.5	58.3	98	99.4	99.4	99.6	99.8
Spontaneous speech	6	12	8	10	12	19	20	20	20	20
Auditory comprehension	90	138	154	129	133	200	194	200	198	198
Repetition	29	70	49	64	57	100	100	97	100	100
Naming	23	54	13	39	48	100	100	100	100	100

2